Arch. Metall. Mater. **71** (2026), 3, 853-859

DOI: https://doi.org/10.24425/amm.2026.1976

ALEKSANDRA BŁONIARZ[1], AGNIESZKA KOPIA[1*]

CORROSION RESISTANCE OF 309S STEEL CMT-CLADDED LAYERS AFTER LONG-TERM EXPOSURE TO BIOMASS

The aim of the research presented was to investigate the influence of different biomass ash at corrosion condition $T = 650°C$ for 2000 h on the surface of weld cladded (CMT) stainless steels 309. The biomass ashes are rich in K_2O, CaO, SiO_2, whereas sewage sludge ash in P_2O_5, CaO, Fe_2O_3 and SiO_2. Characterization of the stainless steel cross-section after the corrosion process inducted by the presence of ash were carried out SEM with EDS analysis. Phase analysis of corrosion products was made by X-ray diffraction (XRD) and simulated using FactSage version 8.3. It has been proved that biomass ashes have the corrosive properties, due to the presence of potassium, and are more aggressive than the sewage sludge ash.

Keywords: Biomass ashes; coatings; steel 309; corrosion; CMT

1. Introduction

Growing environmental concerns, particularly those related to greenhouse gas emissions, have intensified efforts to transition toward more sustainable and environmentally friendly energy sources. In this context, the development and implementation of "green energy" technologies have become essential, not only in energy generation but also in industrial production processes [1-3]. Biomass, derived from organic matter and living organisms, has emerged as a widely available and increasingly utilized alternative to conventional fossil fuels. It encompasses a broad range of materials, including wood, agricultural residues, energy crops, and organic waste. In addition to biomass, sewage sludge represents another promising renewable fuel, offering opportunities for energy recovery through thermal conversion technologies such as pyrolysis, gasification, combustion, and co-combustion [4,5]. These processes are continuously being developed to enhance the efficiency and environmental performance of waste-to-energy systems [6,7]. Despite its advantages, the use of biomass and waste-derived fuels introduces significant technical challenges. One of the primary issues is related to the formation and composition of ash during combustion. Although biomass typically produces less ash than coal, its complex and variable mineralogical composition complicates classification and behavior prediction. The presence of elements such as potassium, sulphur, chlorine, calcium, silicon, and phosphorus contributes to operational problems, including slagging, fouling, bed agglomeration, and high-temperature corrosion [8-10]. High-temperature corrosion is therefore a critical concern in energy systems utilizing renewable fuels [11]. It is strongly influenced by fuel composition, ash chemistry, and operating conditions, especially temperature. Elevated temperatures accelerate chemical reactions and diffusion processes, intensifying material degradation. Among the various forms of degradation, hot corrosion – caused by molten salts in aggressive gaseous environments – poses a particularly severe threat to structural materials. To mitigate these issues, several strategies have been developed, including the application of protective coatings, the use of corrosion-resistant materials, and the addition of chemical inhibitors. Traditionally, low-alloy steels have been employed in boiler construction; however, increasingly aggressive operating conditions have led to a growing use of high-alloy materials and advanced surface engineering techniques [12]. One such technique is Cold Metal Transfer (CMT) [13] welding, which enables the deposition of corrosion-resistant claddings with reduced heat input compared to conventional methods.

In this study, the high-temperature corrosion behavior of weld-cladded from austenitic stainless steel 309, deposited by CMT technique, was investigated in the presence of renewable fuel ashes. The aim of the work is to evaluate the material's resistance to corrosive degradation and to contribute to the development of more durable solutions for energy systems based on renewable fuels.

[1] AGH – UNIVERSITY OF KRAKOW, AL. MICKIEWICZA 30, 30-059 KRAKOW, POLAND

* Corresponding author: kopia@agh.edu.pl

2. Experimental

For the presented study, two types of biomass ashes and sewage sludge ash were used in experiments. The samples were denoted as: OS – oat straw ash, WB – wood biomass ash and SS – sewage sludge ash, respectively. Ash samples were obtain from existing energy units. The chemical composition of ashes is given in TABLE 1. Stainless steels 309 (X15CrNiSi20-12) were weld cladded (CMT technique) on 16Mo3 steel. The samples were cutting from boiler tube (steel 16Mo3) with cladding coating of steel 309. The chemical composition of the investigated 309 steels is given in TABLE 2.

TABLE 1

Chemical composition of the investigated ashes determined after ashing in line with DIN EN ISO 18122 and DIN 51733 [14]

Composition/ wt.%	Wood Biomass (WB) CO_2	Oat Straw (OS)	Sewage Sludge (SS)
CO_2	19,80	7,00	0,00
Na_2O	0,00	0,90	0,53
MgO	8,29	1,98	5,86
Al_2O_3	1,89	0,86	7,55
SiO_2	8,57	33,27	21,00
P_2O_5	7,24	9,67	29,09
SO_3	1,29	2,04	1,85
Cl	0,05	0,57	0,00
K_2O	15,18	36,80	2,26
CaO	34,84	6,47	20,55
TiO_2	0,05	0,05	0,97
Mn	1,91	0,10	0,08
Fe_2O_3	0,90	0,28	1027
Sum	100	100	100
B/A (mass basis)	3,28	1,05	0,5

TABLE 2

Chemical composition of austenitic steels [13]

Type of Steel	Element content, wt. %							
	C	Si	Mn	Cr	Ni	P	S	Fe
309	≤0.22	0.9	2.5	24	13.5	≤0.045	≤0.015	Bal.

To investigate the corrosion products formation in high temperature conditions under the exposure to renewable fuel ashes, samples of steel 309 were covered by OS, WB, SS ashes and placed into the furnace for $t = 2000$ h at $T = 650$°C (Fig. 1).

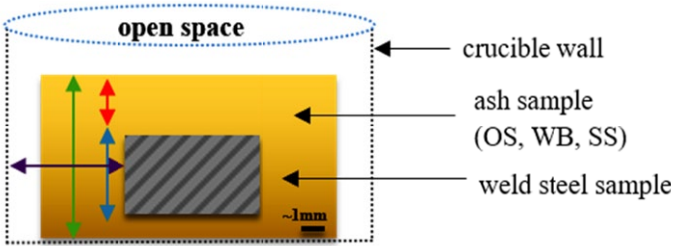

Fig. 1. Scheme of corrosion test equipment (placed inside muffle furnace) [13]

Cross-section of samples were investigated by XRD and SEM-EDS methods. The FEI Quanta 3D FEG Dual Beam microscope was used. SEM-EDS study was also conducted to obtain information about distribution of main elements in the layer which was formed during the process. The samples were observed by secondary electrons using the acceleration voltage in the range of 5-15 kV (surface analysis, cross -section analysis) and 10-20 kV (EDS maps of elements). Phase analysis of corrosion products which occurred on the surface of steel samples was carried out by X-ray diffraction (XRD) using PANanalytical DY-1061EMPTYREAN with CuKα radiation in Bragg-Brentano geometry $2\theta = 20\text{-}80°$; $\lambda_{Cu} = 1{,}54$ Å). Thermodynamic calculations supporting the process of identifying phases formed under given thermodynamic equilibrium conditions were carried out using the FactStage 6.3 program and the FactPS, FToxid and FTsalt databases using the Reaction and Phase Diagram modules. Modules were used to determine the Gibbs free energy ΔG of formation of one oxide mole for steel and ashes and phase equilibrium after tests in ashes at $T = 650$°C in an oxidizing atmosphere.

3. Results and Discussion

The SEM-EDS method allows for investigating the cross-section of corrosion products morphology and chemical composition. Fig. 2 shows the cross-section after the corrosion process with different biomass ashes. These layers seem to be divided into two parts. The layer of corrosion products is inhomogeneous not compact and cracks are visible. The significant difference between the value of the thermal expansion coefficient of the sample substrate and the oxide layer can cause cracks during rapid temperature changes while formation. The thickness of formed

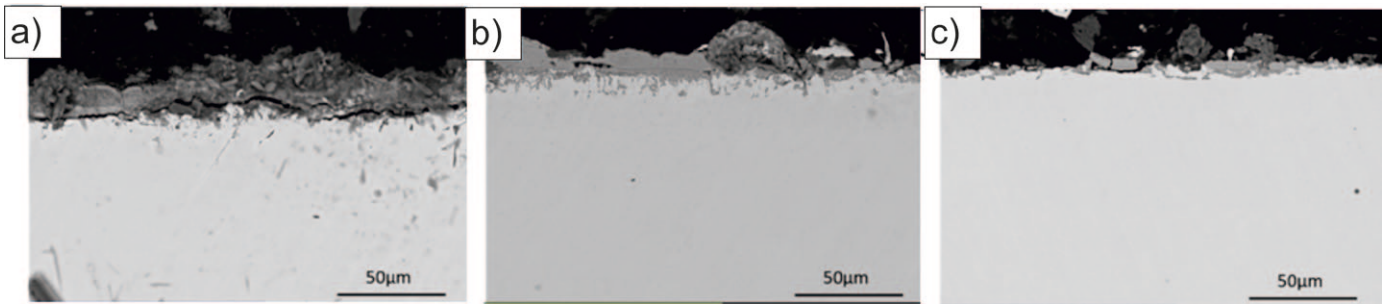

Fig. 2 SEM image of cross-section steel 309 after the corrosion process under a) wood biomass WB, b) oat straw OS, c) sewage sludge SS

layers depends on the type of ash used during the experiment and is in the range of 5-40 µm. The thickest layers on the surface of steel were denoted for samples after exposure to biomass ashes (Fig. 2a, b), while the layer of corrosion products formed during the heating under SS ash was the thinness (Fig. 2c).

On Figs. 3-5 the EDS analysis of investigated coating after corrosion process is presented. After the corrosion tests, the upper layer contains mostly elements from ashes such as K, Cr, Ca, P and Si, while the layer near the steel surface is composed of chromium, nickel and iron oxides. Moreover, iron oxides can be

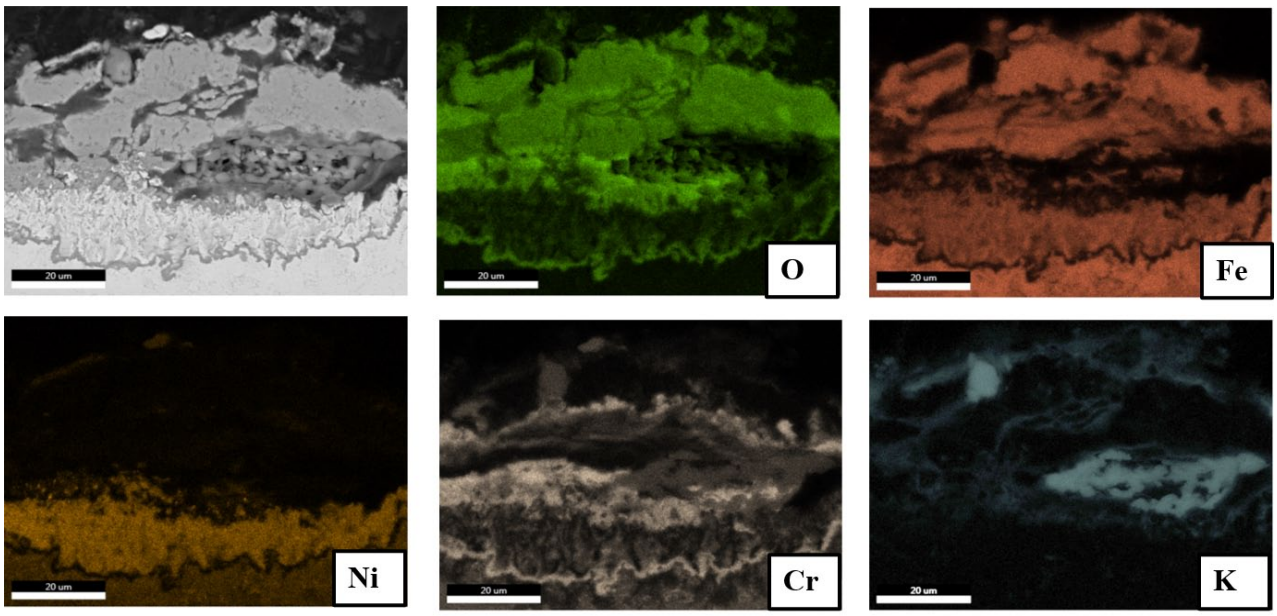

Fig. 3. Map of elements, steel 309 after the corrosion process under oat straw OS ash

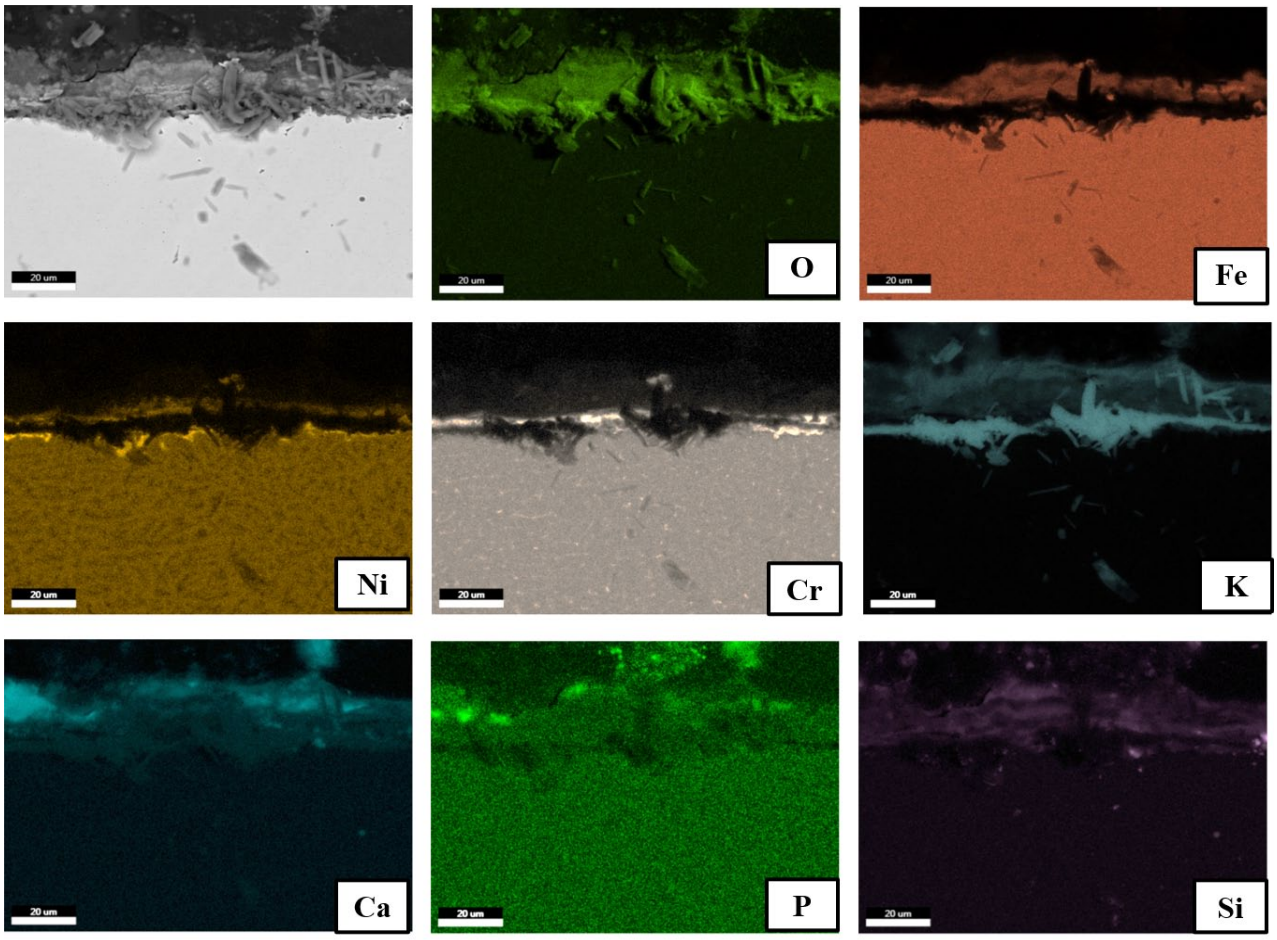

Fig. 4. Map of elements, steel 309 after the corrosion process under wood biomass WB ash

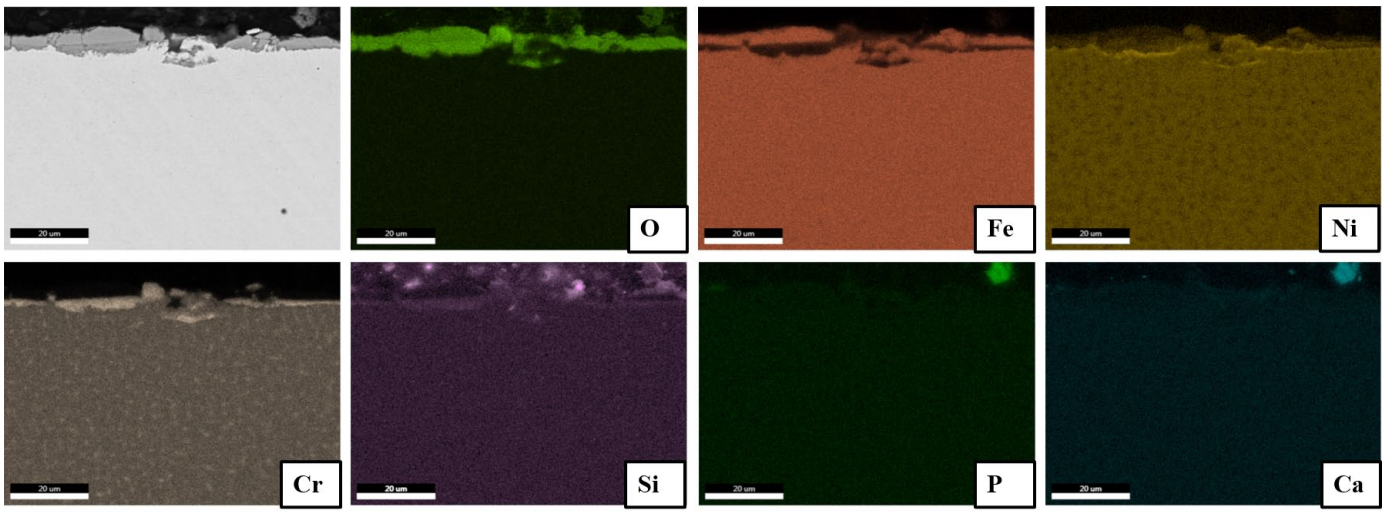

Fig. 5. Map of elements, steel 309 after the corrosion process under sewage sludge SS ash

observed also in the upper layer, thus the diffusion of iron to the surface is not inhibited. In contrast, diffusion of ashes elements into steel is also visible.

Important is phase composition of the corrosion coating. For the identification we used XRD analysis preceded by modeling using FactStage.

Figs. 6-8 present the results of thermodynamic calculations. Modeling showed that during corrosion process in wood ash WB, Cr_2O_3 can only appear at extreme values of oxygen partial pressure, i.e., below 10^{-29} atm. and above 10^{-6} atm. Over the remaining wide range of oxygen partial pressure, chromium forms chromates with ash components, such as potassium chromate (IV) or calcium dichromate (IV) [15]. Additionally, over a wide range of oxygen partial pressure, it occurs in the form of spinel with iron, $FeCr_2O_4$. Iron forms oxides Fe_2O_3 and Fe_3O_4 and can also form a phase with phosphorus, $FePO_4$. The main ash elements are potassium and calcium, which can also form K_2SiO_3, $K_2Si_2O_5$, or $K_2Si_4O_9$ phases [16]. Calcium has a greater affinity for phosphorus, which can form $Ca_3(PO_4)_2$ and $Ca_2P_2O_7$ phases. Residues of phases constituting ash may also appear in the system. Similar phases are formed in the oat straw biomass with 309 cladding coating system. Differences phases are observed in system 309 sewage sludge ash. Cr_2O_3 occurs at oxygen partial pressures below 10^{-29} atm. and above 10^{-7} atm. In the remaining range, it forms spinel $FeCr_2O_4$. Iron forms oxides Fe_2O_3 and Fe_3O_4, as well as compounds with ash components

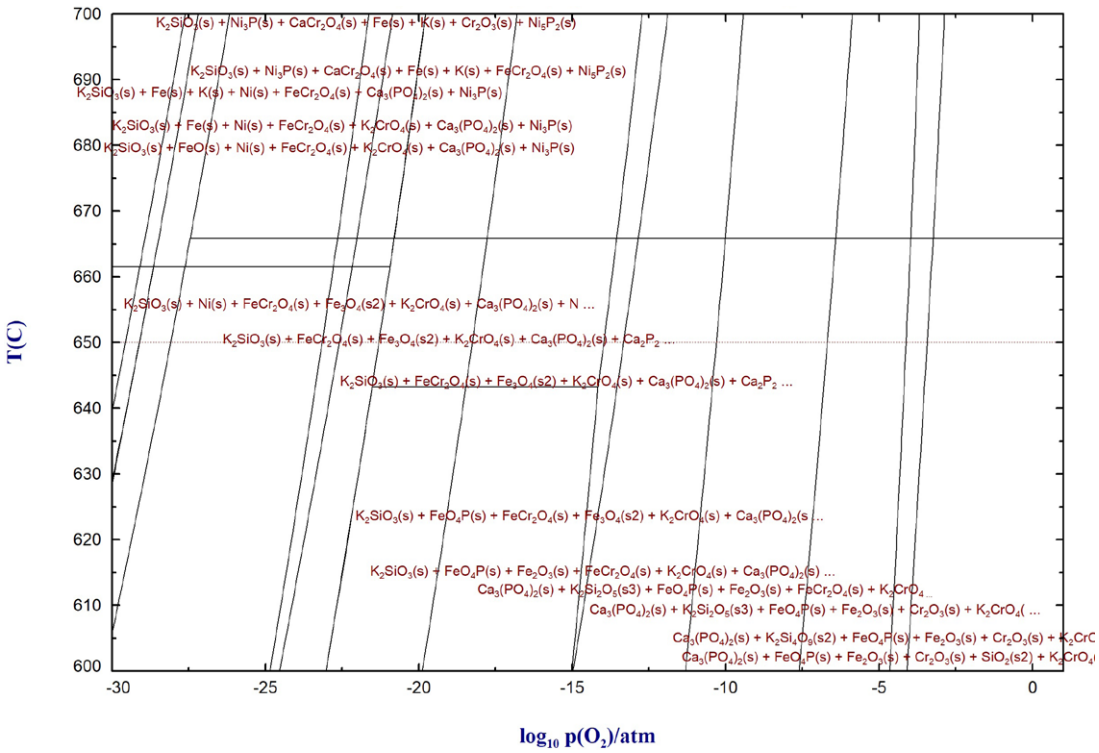

Fig. 6. The Fe – Cr – Ni – K – Ca – Si – P – oxygen phase diagram for the 309S steel coating heated in the presence of mixed wood ash

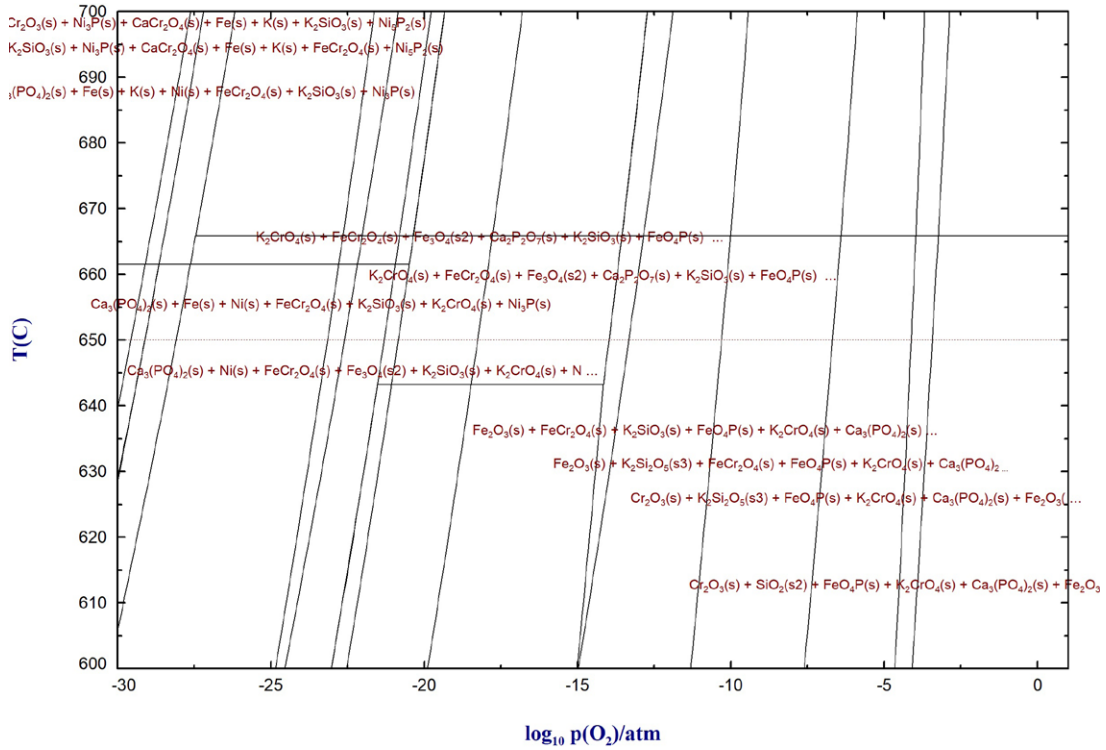

Fig. 7. Fe – Cr – Ni – K – Ca – Si – P – oxygen phase diagram for the 309S steel coating heated in the presence of oat straw ash

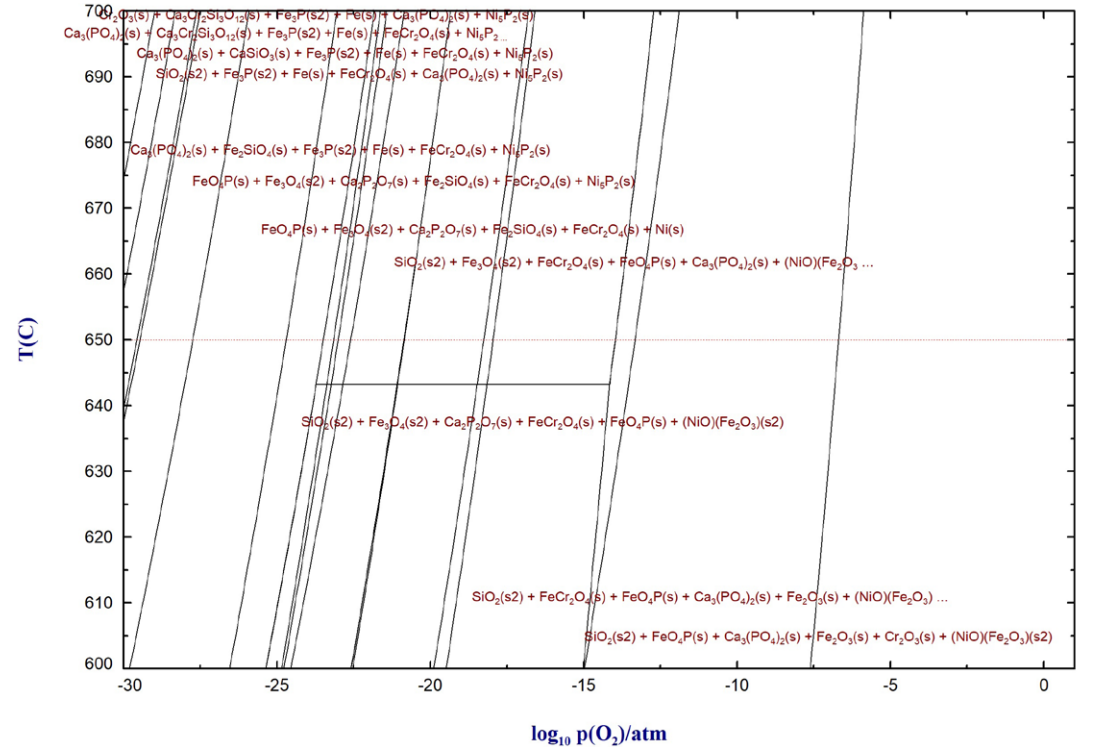

Fig. 8. Fe – Cr – Ni – K – Ca – Si – P – oxygen phase diagram for the 309S steel coating heated in the presence sewage sludge ash

Fe_2SiO_4, $FePO_4$, and Fe_3P. Nickel, in addition to its oxide, can form a phase with phosphorus Ni_5P_2. Calcium, as in other ashes, forms phosphates $Ca_3(PO_4)_2$ and $Ca_2P_2O_7$, and silicates $CaSiO_3$. The ash component SiO_2 is also an additional phase.

XRD analysis for all samples of steel 309 under the WB, OS and SS ash are presented on Fig 9. For samples heated in the WB and OS process, the main phases are Fe_2O_3, $FeCr_2O_4$, K_2CrO_4, and $Ca_3(PO_4)_2$, $Ca_2P_2O_7$, NiO and Ni_3P. For samples heated in the SS ash we identify the phases SiO_2, Fe_2O_3 and $Ca_3(PO_4)_2$ main phases of the ash.

The obtained XRD analysis results are in accordance with the modeling performed using the FactStage program.

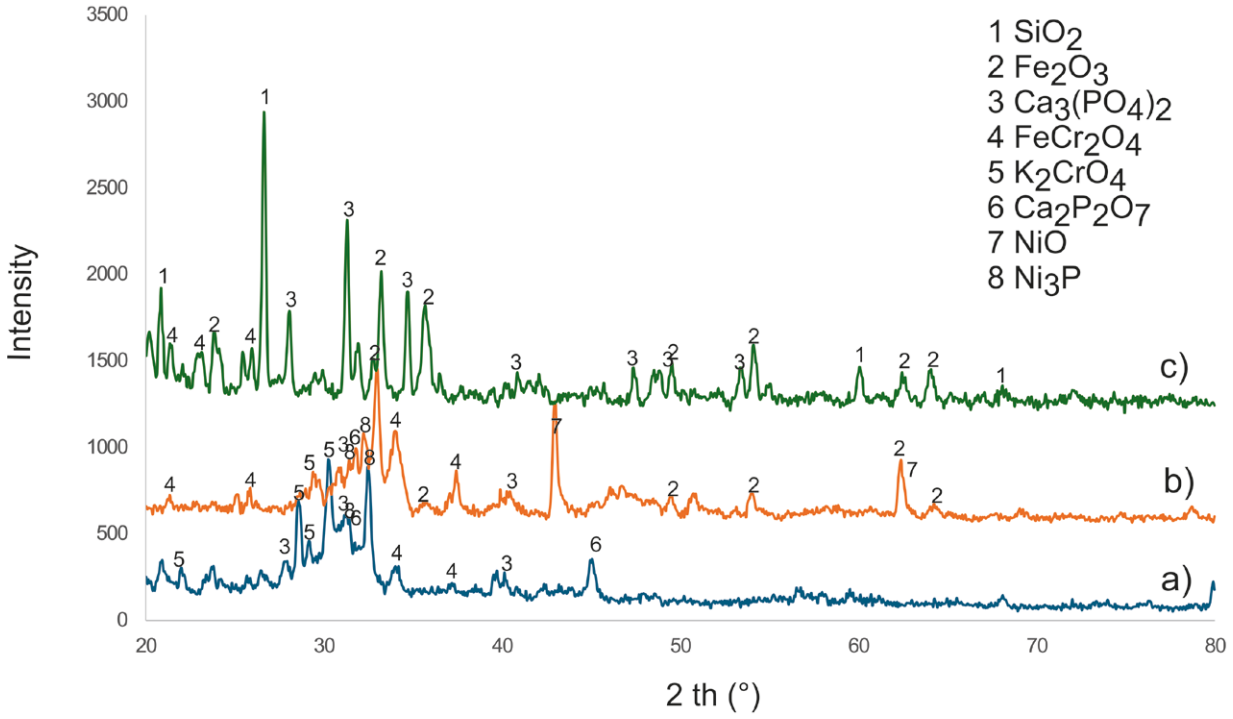

Fig. 9. XRD patterns of 309 steel after the corrosion process under a) WB, b) OS, c) SS the phase composition: 1- SiO_2, 2-Fe_2O_3, 3-$Ca_3(PO_4)_2$, 4- $FeCr_2O_4$, 5-K_2CrO_4 ,6-$Ca_2P_2O_7$, 7-NiO, 8- Ni_3P

4. Conclusion

In the presented work weld cladded (cold metal transfer method) from 309 austenitic stainless steels coating was investigated after the exposure to renewable fuel ashes such as biomass ashes (oat straw and wood biomass), as well as sewage sludge ash in high temperature. The experiment performed using $t = 2000$ h and $T = 650$°C. The layer of corrosion products formed after the exposure to ashes depends mostly on kind renewable fuel ashes. The thickest layers on the surface of steel were observed for samples after exposure to biomass ashes and the thinner layer was for sewage sludge ash. The thickness of corrosion products layer was in the range of 5-40 µm. Furthermore, there were visible cracks and inhomogeneous layers. XRD and SEM-EDS analysis supported by FactStage 6.3 program show the phases composition of the corrosion layers and indicate which elements in the ash are highly corrosive and destroy the protective layer of the steel coating. In the case of WB and OS ash, this element is potassium, which has a strong affinity for chromium. This element affects the degradation of the protective Cr_2O_3 coating, forming potassium chromates (IV) K2CrO4 phase. In the case of SS ash, none of the elements in the ash exhibits an affinity for chromium. Although Ca is present in this ash, which could be aggressive and form the chromate (VI). In this case form in a wide range as phosphate – $Ca_3(PO4)_2$, $Ca_2P_2O_7$. Based on the obtained results and thermodynamic data, it can be concluded that Ca, an alkali metal, does not pose a threat to the protective Cr_2O_3 layer, as it forms phases with phosphorus due to its high affinity for phosphorus. Taking the above into account, for applications where OS and WB type biomass is burned, the material for the devices should be selected very consciously in terms of corrosion resistance in the presence of potassium**.**

Acknowledgment

This work was supported by the Polish Ministry of Science and Higher Education and statutory funds of the AGH University of Krakow.

REFERENCES

[1] R. Trabelsi, Impact of renewable and fossil energy on sectoral CO_2 emissions: empirical evidence from the United States and China. Discover Sustainability **6**, 1448 (2025).

[2] V.K. Sharma, G. Monteleone, G. Braccio, C.N. Anyanwu, N.N. Aneke, Comprehensive Review of Green Energy Technologies: Tow. Sust. Clean Energy Tran. Global Net-Zero Carb. Emi. Processes **13** (69), (2025). DOI: https://doi.org/10.3390/pr13010069

[3] R. Jayabal, Towards a carbon-free society: Innovations in green energy for a sustainable future. Res. Engin. **24**, 103121 (2024). DOI: https://doi.org/10.1016/j.rineng.2024.103121

[4] Z. Luo, J. Zhou, Ther. Conver. of Biom.; Handbook of Clim. Chan. Mitig. Adap. Springer, (2025).

[5] A. Magdziarz, M. Wilk, M. Gajek, D. Nowak-Woźny, A. Kopia, I. Kalemba-Rec, J.A. Koziński, Properties of ash geneated during sewage sludge combustion: A multifaceted analysis. Energy **113**, 85-94 (2016). DOI: https://doi.org/10.1016/j.energy.2016.07.029

[6] M. Sieradzka, A. Mlonka-Mędrala, A. Błoniarz, A. Magdziarz Experimental study of biomass waste gasification: impact of atmosphere and catalysts presence on quality of syngas production. Biores. Techn. **394**, 1-10 (2024).
DOI: https://doi.org/10.3390/en15103539

[7] A. Zhou, N. Deng, S. Deng, Z. Hu, A. Magdziarz, H. Tan, X. Wang, Study on pyrolysis behavior of municipal sludge based on TG-FTIR-MS. J. of the Ener. Inst. **114**, 1-8 (2024).
DOI: https://doi.org/10.1016/j.joei.2024.101643

[8] Y. Kawahara, High temperature corrosion mechanisms and effect of alloying elements for materials used in waste incineration environment. Corros. Sci. **44**, 223-245 (2002).
DOI: https://doi.org/10.1016/s0010-938x(01)00058-0

[9] R.A. Antunes, M.C.L. de Oliveira, Corrosion in biomass combustion: A materials selection analysis and its interaction with corrosion mechanisms and mitigation strategies. Corros. Sci. **76**, 6-26 (2013). DOI: https://doi.org/10.1016/j.corsci.2013.07.013

[10] I. Obernberger, T. Brunner, G. Barnthaler, Chemical properties of solid biofuels – significance and impact. Biom. Bioen. **30**, 973-982 (2006). DOI: https://doi.org/10.1016/j.biombioe.2006.06.011

[11] X. Wu, L. Li, B. Li, Z. Wang, Y. Wu, Current status and future trends of high-temperature gas environment corrosion on metal coatings in solid waste incinerators. Proc. Saf. Environ. Prot. **191**, 146-162 (2024. DOI: https://doi.org/10.1016/j.psep.2024.08.116

[12] K. Khantisopon, S. Singh, J. Jitputti, Ch.C. Berndt, A.S.M. Ang, High Temperature Corrosion Resistant and Anti-slagging Coatings for Boilers: A Review. High Temp. Corr. of Mat. **101**, S1-S55 (2024).
DOI: https://doi.org/10.1007/s11085-024-10251-0

[13] A. Dębowska, A. Magdziarz, A. Kopia, I. Kalemba-Rec, P. Petrzak, Influence of fuel ashes on corrosion of surface coatings cladded by CMT method. Ener. Sour. Pt. A, **41** (4), 427-437 (2019).
DOI: https://doi.org/10.1080/15567036.2018.1520327

[14] A. Błoniarz, M. Schreiner, M. Reinmöller, A. Kopia, Corrosion Resistance of Inconel 625 CMT-Cladded Layers after Long-Term Exposure to Biomass and Waste Ashes in High-Temperature Conversion Processes. Materials **13**, 4374 (2020).
DOI: https://doi.org/10.3390/ma13194374

[15] J. Pettersson, N. Folkeson, L. G. Johansson, J. E. Svensson, The effects of KCl, K_2SO_4 and K_2CO_3 on the high temperature corrosion of a 304-type austenitic stainless steel. Oxid. Met. **76**, 93-109 (2011).
DOI: https://doi.org/10.1007/s11085-011-9240-z

[16] A. Mlonka-Mędrala, A. Magdziarz, I. Kalemba-Rec, W. Nowak, The influence of potassium-rich biomass ashes on steel corrosion above 550°C. Ener. Convers. Manag. **187**, 15-28 (2019).
DOI: https://doi.org/10.1016/j.enconman.2019.02.074